ADVANCED FUNCTIONAL MATERIALS
www.afm-journal.de

The Formation of Residual Lithium Compounds on Ni-Rich NCM Oxides: Their Impact on the Electrochemical Performance of Sulfide-Based ASSBs

Burak Aktekin, Alexander E. Sedykh, Klaus Müller-Buschbaum, Anja Henss, and Jürgen Janek**

Residual lithium compounds (RLCs) are known to form on the surface of nickel-rich $LiNi_{1-x-y}Co_xMn_yO_2$ (NCM) oxides during synthesis and storage. In this study, the impact of RLCs on cathode performance in sulfide-based all-solid-state batteries (ASSBs) is investigated by employing practically relevant approaches to generate (or remove) RLCs on (or from) NCM single crystal particles. It is revealed that Li_2CO_3 is the predominant component in samples exposed to air. Surprisingly, heat treatment at high temperatures does not remove RLCs but increases the overall RLC content, accompanied by the partial transformation of existing RLCs into Li_2O. These samples exhibit compromised electrochemical performance due to asymmetric overpotential increase during cell discharge. However, it is possible to recover performance through controlled ambient air storage which enables the conversion of existing Li_2O into Li_2CO_3 and formation of fresh Li_2CO_3 on the surface. Notably, the beneficial effects are not replicated with pure CO_2 or moisturized air storage, emphasizing the significance of storage conditions and reaction pathways for Li_2CO_3 formation. This study demonstrates that removal of Li_2O residuals through the formation of Li_2CO_3 under controlled ambient air exposure proves to be advantageous for sulfide-based ASSBs, thereby offering valuable guidance for the development of optimized NCM-based ASSB systems.

1. Introduction

Lithium-ion batteries (LiBs) are expected to play a central role in electrification of transport in the near future.[1] The development of advanced positive electrode (cathode) materials, i.e., cathode active materials (CAMs), is quite critical for accelerating the transition from internal combustion engines to electric vehicles. Today, nickel-rich $LiNi_{1-x-y}Co_xMn_yO_2$ (NCM) layered oxides are considered as one promising group of CAM due to their high specific charge capacity (>200 mAh g^{-1}) and high redox potential.[2] During their synthesis, it is a common practice to use an excess amount of lithium precursor (e.g., LiOH, Li_2CO_3) since this helps to compensate for lithium loss during high temperature calcination and inhibits cation disorder in the CAM crystal structure.[3] As a result, residual lithium compounds (RLCs), e.g., LiOH and Li_2CO_3, are commonly present on the CAM surface. As compared to other CAMs such as olivine-type $LiFePO_4$ (LFP) and spinel-type $LiNi_{0.5}Mn_{1.5}O_4$ (LNMO) oxides, nickel-rich NCMs are also known to be highly sensitive toward ambient air exposure.[4–6] Their reactivity toward moisture and CO_2 in air results in formation of RLCs.[7,8] Therefore, the handling of nickel-rich CAM powders requires controlled atmosphere in order to prevent formation of RLCs – and associated lithium loss from the CAM crystal lattice.

B. Aktekin, A. Henss, J. Janek
Institute of Physical Chemistry
Justus-Liebig-Universität Giessen
D-35392 Giessen, Germany
E-mail: burak.aktekin@phys.chemie.uni-giessen.de;
juergen.janek@phys.chemie.uni-giessen.de

The ORCID identification number(s) for the author(s) of this article can be found under https://doi.org/10.1002/adfm.202313252

DOI: 10.1002/adfm.202313252

B. Aktekin, K. Müller-Buschbaum, A. Henss, J. Janek
Center for Materials Research
Justus-Liebig-Universität Giessen
D-35392 Giessen, Germany

A. E. Sedykh, K. Müller-Buschbaum
Institute of Inorganic and Analytical Chemistry
Justus-Liebig-Universität Giessen
D-35392 Giessen, Germany

In liquid electrolyte-based LiBs, the impact of RLCs on the cell performance has been in the focus of numerous studies in recent years.[9] During the preparation of positive electrode sheets, RLCs increase the pH of the slurry and cause gelation due to decomposition of commonly used binder material polyvinylidene fluoride (PVDF).[10,11] Besides, during cell operation, RLCs can be decomposed and cause electrolyte side reactions. For instance, Li_2CO_3 can be decomposed at 3.8 V versus Li^+/Li by forming CO_2 and CO gaseous products[12] and reactive oxygen species.[13] Indirect (chemical) decomposition of Li_2CO_3, which can be induced by the protons formed by electrolyte oxidation reactions, has also been proposed.[14] In either case, oxidation of Li_2CO_3 could result in formation of gaseous species or deposition of electrolyte side reaction products. In addition to these, formation of RLCs during ambient air storage is also associated with near-surface structural changes of CAMs, e.g. rock-salt phase transformation.[15–18] These aforementioned problems, encountered either during electrode manufacturing or cell operation, negatively affect the electrochemical performance of LiBs consisting of Ni-rich layered oxide CAMs. Therefore, post-synthesis processes such as washing and thermal treatment (under different atmospheres) are usually applied to nickel-rich CAMs to remove the RLCs and to mitigate aforementioned problems[8] even though these processes may lead to further issues, e.g. Li^+/H^+ exchange during water washing and near-surface structural damage.[16,19] Optimization of washing solutions via pH-control or the use of alternative solvents (e.g., anhydrous ethanol or methanol) can reduce the damage from washing procedure,[7,9,20] however, it is important to account for the cost implications.

In the case of all-solid-state batteries (ASSBs), the electrode manufacturing process and therefore the microstructure of the cathode differ considerably from conventional porous electrodes for LiBs. Pellet-type electrode preparation (for lab-scale research) is a dry process. In the case of sheet-type electrode preparation, slurry-based processing or in situ polymerization have been explored, while dry electrode preparation processing is recently targeted for future applications (e.g., sulfide SEs).[21–23] On the one hand, the presence of basic RLCs on CAM particles does not pose the same problem like in the case of liquid electrolyte LiBs (i.e., slurry gelation). On the other hand, the mechanical properties of the solid electrolyte (SE) make the composite electrode more susceptible to CAM |SE contact issues. The presence of ionically and electronically almost insulating RLCs (e.g., Li_2CO_3) may exacerbate the ionic and electronic resistance issues, and therefore impair the electrochemical performance.[24] If RLCs get oxidized and form gaseous products,[25–27] it is reasonable to expect a further increase of contact resistances since SE particles cannot fill the formed cavities like its liquid counterparts. As a positive effect, in ASSBs with sulfide SEs, surface carbonates have been reported to be acting like a protective buffer layer between the CAM and SE, and therefore, are considered to be beneficial to the electrochemical performance.[28–31] For this reason, we consider it as important to understand which RLCs are formed on nickel-rich layered oxide CAMs during the synthesis and storage, and how they affect the electrochemical performance in ASSBs.

In this study, driven by the existing knowledge gap regarding the impact of various types of RLCs on ASSB performance, we have comprehensively investigated the formation of RLCs on the surface of single crystalline $LiNi_{0.83}Mn_{0.06}Co_{0.11}O_2$ powders which were subjected to different thermal treatments and were stored under different gas atmospheres. The relationship between different RLCs and electrochemical performance of ASSB cells is evaluated with Li_6PS_5Cl (lithium argyrodite) SE. Our results show that the type of RLC is more decisive than the amount of RLCs present on Ni-rich NCM powders. The formation of Li_2O in the final heat treatment during NCM synthesis is shown to be detrimental to the electrochemical performance of sulfide-type ASSB. The fast capacity fading of cells with Li_2O as the major RLC is mainly caused by an asymmetric overpotential evolution during the cell discharge (i.e., lithiation of the CAM). Our results show that a controlled exposure of NCM powders to ambient air enables complete conversion of residual Li_2O to Li_2CO_3 and also forms fresh Li_2CO_3 on the surface through minor delithiation of the NCM, improving the cell performance considerably. This is in stark contrast to the processing of CAM for LIBs with liquid electrolytes and highlights the specific requirements of ASSBs.

2. Results and Discussion

2.1. Removal of RLCs by washing

To understand how RLCs affect the electrochemical cathode performance in a sulfide-type ASSB, we first aimed to prepare an optimal "reference" NCM sample. For this, we removed any pre-existing RLCs from the as-received powders. According to estimates from acid titration analysis (see Figure S1, Supporting Information), the pristine powders had ≈0.17 wt% LiOH and 0.3 wt% Li_2CO_3 on their surface (corresponding to a charge of ≈4.1 mAh g^{-1} as normalized to the CAM mass). It is seen from the C 1*s* XPS spectra (**Figure 1a**) that carbonates are present on the pristine CAM surface and that they were removed successfully (Figure 1b) after water washing (3 min washing followed by 100 °C vacuum drying).

Previously, the presence of basic nickel carbonates, e.g. $NiCO_3{\cdot}2Ni(OH)_2{\cdot}xH_2O$, has been proposed to be the major surface contaminant on nickel-rich NCM CAMs formed during air storage.[36] However, this compound is insoluble in water,[37] and therefore removal by water washing is unlikely. Normalized Li 1*s* and Ni 2*p* XPS spectra (normalized with respect to the NCM-related metal oxide peak in O 1*s*) suggest that the carbonate species present on the NCM-surface (which were removable by water washing) are mainly lithium carbonates rather than basic nickel carbonates since the Li 1*s* peak intensity decreases after washing while the Ni 2*p* peak intensity increases (see Figure S2, Supporting Information). MP-AES elemental analysis of washing solutions corroborated these findings as it shows that the amount of lithium is in good agreement with the value determined by the acid titration (1.56 and 1.62 mg L^{-1}, respectively) while the amount of nickel in the washing solution was negligible.

Electrochemical testing of unwashed and washed samples in In/InLi | LPSCl | NCM cells shows that the effect of washing was quite significant, and it resulted in a worse cell performance (see Figure 1c,d). Already at a low cut-off voltage (3.1 V vs In/InLi, i.e., 3.7 V vs. Li^+/Li), the overpotential of the washed sample was rather large and caused a substantial drop in charge and discharge capacities. XRD results do not indicate any bulk structural change (see Figure S3, Supporting Information), therefore, the

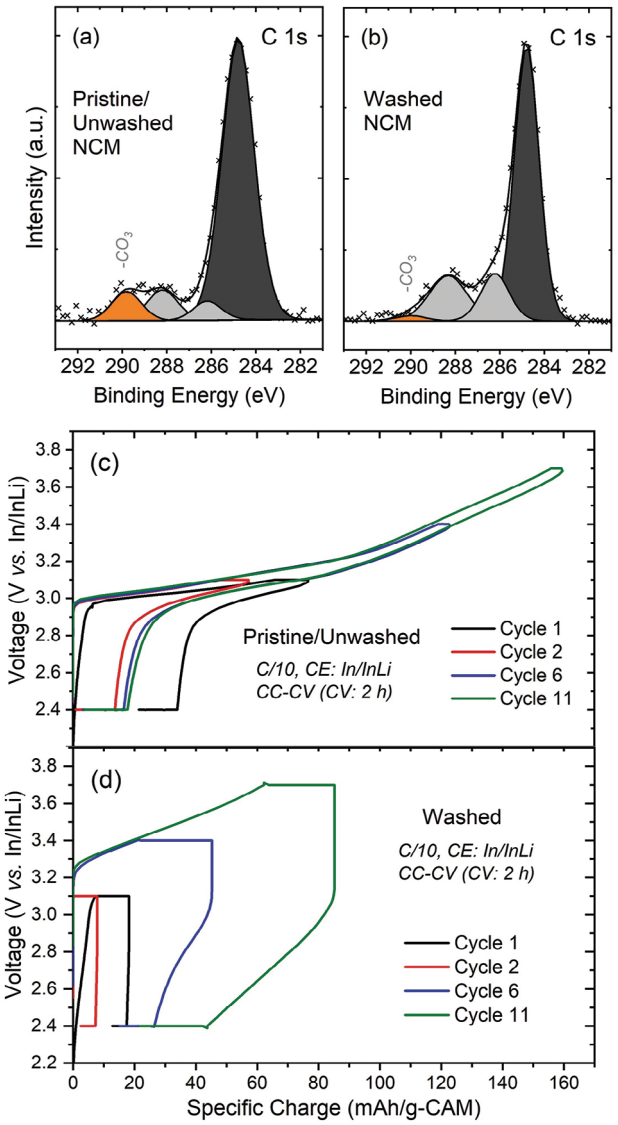

Figure 1. Normalized C 1s XPS spectra of nickel-rich NCM powders before a) and after b) short duration water washing. Galvanostatic cycling of In/InLi-NCM cells with c) non-washed and d) washed nickel-rich NCM powders. In order to see the effect of the cathode potential on the cell overpotential, the upper cut-off voltage was gradually increased every 5 cycles.

performance difference likely originates from the near-surface changes of the CAM, as XRD is not a surface sensitive technique.

Subsequent high temperature annealing of washed NCM powder at 650 °C (under pure oxygen flow) also did not help to recover its electrochemical performance (see Figure S4, Supporting Information). In previous reports, water exposure of NCM powders, and as a result, Li^+/H^+ exchange near the CAM surface have been shown to result in oxygen-release and associated near-surface structural transformations (e.g., spinel/rock-salt phase formation) during the subsequent annealing process.[16,19] Delithiated nickel-rich NCM is known to have a very low thermal stability[38] and these phase transformations can take place already during the powder drying process (typically run at 100 °C under vacuum). Therefore, it is reasonable to expect structural

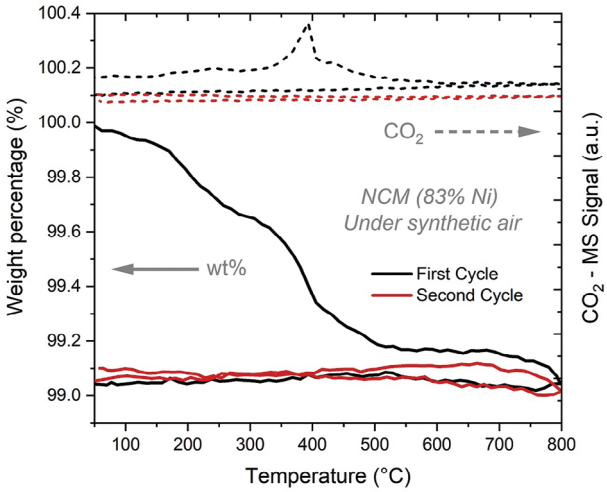

Figure 2. TGA-MS results of pristine nickel-rich NCM powders during subsequent cycles of heating/cooling (under CO_2/moisture-free, argon-diluted synthetic air conditions).

damage and deteriorated electrochemical performance after secondary washing procedures in agreement with the electrochemical cycling results in Figure 1c,d and Figure S4 (Supporting Information). In a recently published study, a notably negative impact of washing has been reported (in agreement with our observations), however, this behavior was attributed to the absence of protective RLCs on the surface.[31] However, in the light of the surface damage concerns mentioned previously, the focus in this study is directed to alternative approaches (e.g., heating) which potentially can minimize the damage to the sample surface while obtaining an RLC-free reference sample.

2.2. Removal of RLCs by high temperature heat treatment

The removal of surface carbonates at high temperatures by thermal decomposition has been proposed in earlier studies.[18,25,36,39,40] Considering the fact that such heat treatments are also commonly applied to NCM powders during/after their synthesis, it is reasonable to use this approach in order to obtain RLC-free reference samples. However, due to low thermal stability of nickel rich NCM, the choice of heat treatment conditions is important since structural damage via oxygen release from the lattice is possible at high temperatures. Therefore, in order to determine a suitable temperature for heat treatment, the thermal behavior of CAM powder during two consecutive heating and cooling cycles under synthetic air conditions (with the exclusion of CO_2 and moisture) was investigated and the results are shown in **Figure 2**.

Figure 2 shows that a considerable weight loss starts at ≈150–200 °C which can be due to thermal decomposition of surface contaminants such as chemisorbed water (e.g., $LiOH{\cdot}H_2O$)[36] and adsorbed bicarbonate and carbonate species.[41] Even though a slight increase in CO_2 signals is observed in this temperature range, much stronger CO_2 signals become visible at 370 °C and it is accompanied by a sharp decline in the sample mass. Similar CO_2 evolution trends were observed in previous reports,[36,37,41] however, Sicklinger et al.[36] suggested the

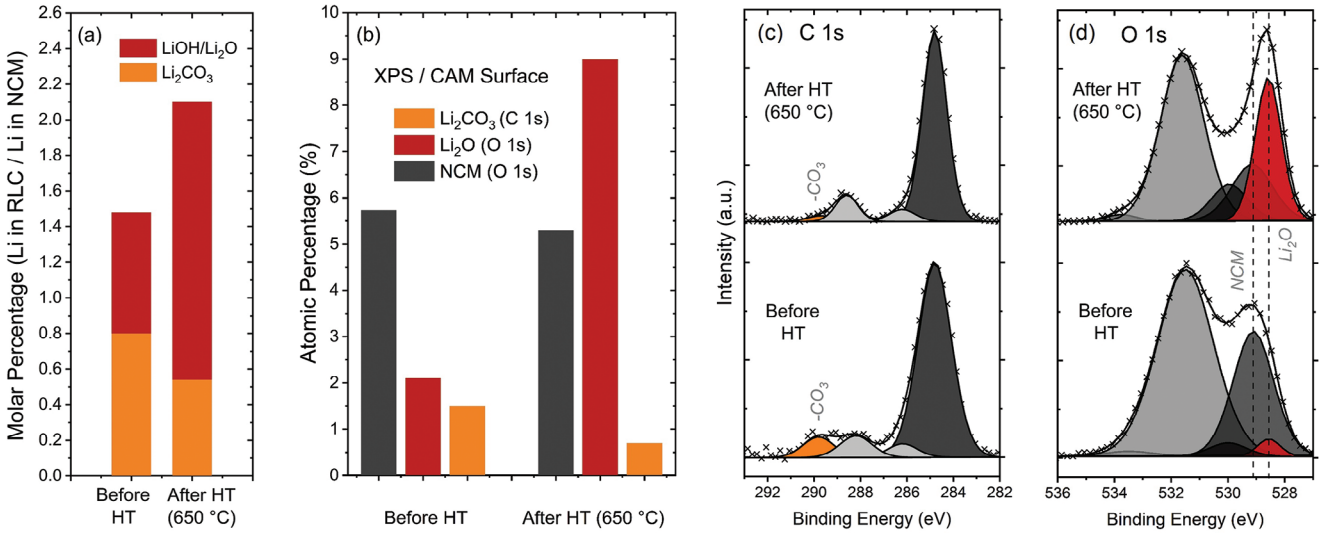

Figure 3. a) Acid titration results of NCM powders before and after the heat treatment (650 °C, under pure oxygen flow). b) Comparative surface atomic percentage trends for Li_2CO_3, Li_2O and NCM as obtained from C 1s and O 1s XPS results. c) C 1s and d) O 1s normalized XPS spectra of NCM powders before and after the heat treatment.

decomposition of basic nickel carbonates to explain the CO_2 release observed at such low temperatures. Based on our observations of acid titration, XPS and MP-AES measurements (as discussed in the previous section), we assume that thermal decomposition of basic nickel carbonates does not make a considerable contribution to the observed CO_2 release for the samples used in this study (i.e., $LiNi_{0.83}Mn_{0.06}Co_{0.11}O_2$ single crystalline powders). Interestingly, thermal decomposition behavior in this range (< 550°C) seems also to change depending on the formation pathways of carbonates (see Figure S5, Supporting Information).

The decrease in sample weight ceases at temperatures above 550 °C, and the weight stays nearly constant until the temperature approaches ≈680 °C. Above this temperature, the weight starts to decrease gradually (it should be noted that the changes in this region are at the limits of the instrument yet discernible over two consecutive cycles). Oxygen release from the layered NCM and thus phase transformations (e.g., spinel and rock-salt phase formation) are expected in this temperature range (>680 °C).[36,37] Thermal decomposition of bulk-Li_2CO_3 reference samples were also reported at similar temperatures,[36] however, no CO_2-MS signals are observed in Figure 2 for this temperature region, indicating that the oxygen release from the NCM lattice is mainly responsible for the decrease of weight. This is further corroborated by a similar TGA-MS measurement performed under argon atmosphere (see Figure S6, Supporting Information) which shows a more significant weight decrease in this region due to the much lower oxygen partial pressure in pure argon gas as compared to synthetic air. Based on these observations, heat treatment at 650 °C in a pure oxygen atmosphere was selected with the aim of preventing or minimizing near-surface structural damage to NCM powder during the removal of RLCs.

The acid titration results of the CAM powders (see Figure S7, Supporting Information) show that the total amount of RLCs increases from 4.1 to 5.8 mAh g^{-1} after 650 °C heat treatment in oxygen atmosphere (charge equivalent of lithium present in RLCs is given as normalized to the CAM mass for an easier interpretation of cycling results). On the other hand, the percentage of Li_2CO_3 decreases to 0.2 wt% from 0.3 wt% while the percentage of LiOH increases to 0.38 wt% from 0.17 wt%. Although there may be some uncertainty in these estimates due to factors such as additional lithium leaching during washing, or presence of trace amount of CO_2 in the analyte,[4,7] both measurements were performed carefully with an identical methodology. Thus, the trends in **Figure 3a** clearly indicate that the Li_2CO_3 residuals partially transform into other RLCs instead of re-lithiating NCM (similar trends were also observed at 750 and 800 °C). It should be noted that Li_2O reacts with water by forming LiOH as the reaction product. However, the acid titration is a pH-based technique and water is used in the analyte. Therefore, quantification results for LiOH could also be caused by Li_2O present on the NCM surface. Indeed, the C 1*s* XPS results of heat-treated powders show that the carbonate-related peak intensity significantly decreases (see Figure 3c) after the heat treatment while a strong new peak emerges in O 1s spectrum at a binding energy of 528.6 eV corresponding to Li_2O (see Figure 3b–d). Formation of residual Li_2O on nickel rich NCM surface during the synthesis is expected,[3,42,43] and it is shown that it also forms during the heat treatment at 650 °C under oxygen flow.

In this work, the heat treatment was performed under pure oxygen flow and afterwards the samples were transferred into the glovebox as quick as possible (maximum 1 and 2 min of air exposure) to minimize air exposure. It is known that Li_2O is reactive toward H_2O[44] and CO_2.[45] Therefore, the ambient air exposure/storage of nickel rich NCM powders is not only expected to result in RLC formation directly on NCM surface, but also to transform Li_2O residuals possibly present on the surface into LiOH and Li_2CO_3. Thus, it is important to understand the reaction kinetics of Li_2O residuals on the surface – as well as the reaction kinetics of the NCM itself – since the surface properties could significantly affect the interphase

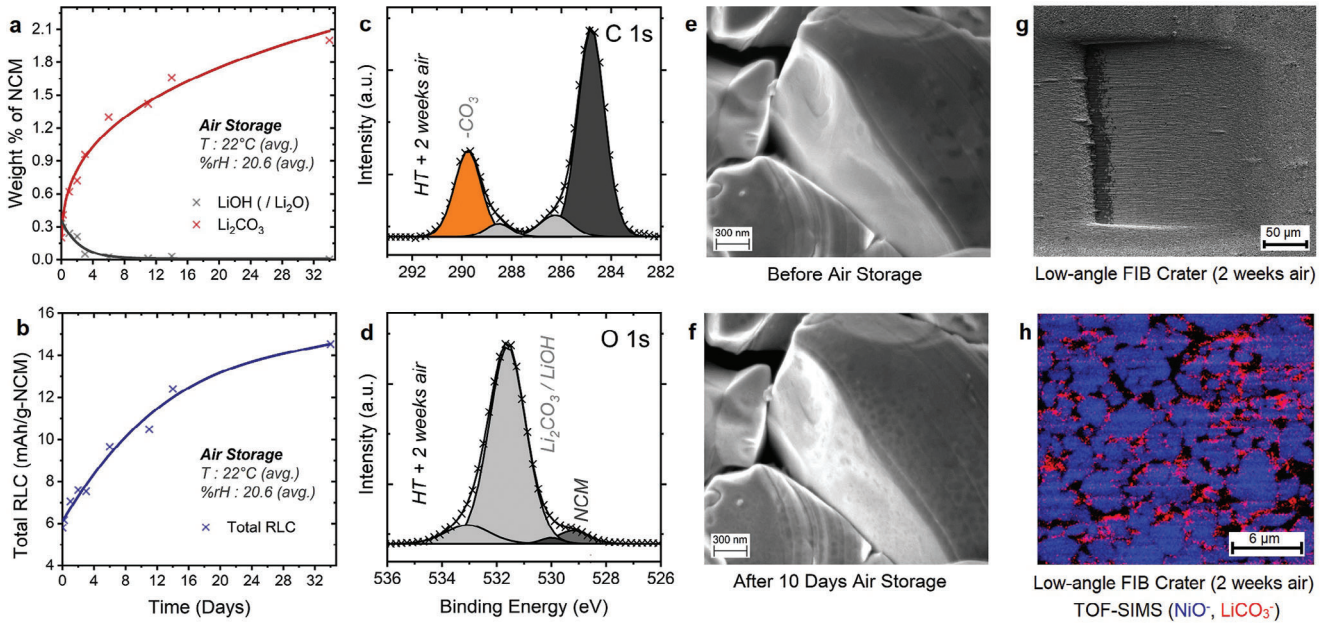

Figure 4. a,b) Acid titration results of heat treated NCM powders (heat treated at 650 °C under pure oxygen flow) after exposure to ambient air atmosphere for different durations. c,d) C 1*s* and O 1*s* XPS spectra of heat treated NCM powders after 2 weeks air exposure. e,f) SEM images of NCM powders before and after 10 days air exposure. For a better comparison, NCM powders were not removed from the SEM sample holder during the air exposure and the exact same spot was used for imaging after 10 days. g) A low-angle (≈10° from the sample surface) FIB crater was cut into NCM powder (exposed to air for two weeks) using a xenon plasma. For the crater preparation, the powders were initially hand-pressed on aluminium foil substrate. h) ToF-SIMS image of the low-angle crater formed on the two-weeks air exposed sample. In the image, NiO^- ion signals are shown in blue and $LiCO_3^-$ ion signals are shown in red.

evolution during the electrochemical cycling and thus the cell performance.

2.3. Ambient air exposure

The effects of ambient air exposure on RLC formation (and transformation) were studied over the duration of nearly one month following the initial heat treatment at 650 °C under pure oxygen flow. As seen in **Figure** 4a and b, the amount of LiOH (mostly originating from Li_2O on the NCM surface) quickly decreases and its weight percentage reaches near zero in already three days. In the same time interval, the amount of Li_2CO_3 shows a rapid increase in weight fraction. Through the rest of the storage, the total amount of RLCs continues to increase gradually with a corresponding increase in the Li_2CO_3 amount. The XPS analyses of powders exposed to air for two weeks (Figure 4c and d) show that the carbonate-related peak in the C 1*s* spectrum increases significantly in intensity while at the same time the Li_2O-related peak in O 1*s* spectrum completely disappears. It is also seen that the relative intensity of the metal oxide peak (i.e., from the NCM lattice) decreases noticeably due to formation of carbonates on the NCM-surface. Island-like formation of RLCs also become visible with electron microscopy as shown in Figure 4e and f as round-shaped dark regions appear on the NCM surface after 10 days of air exposure. Previously, negative ToF-SIMS ion fragments such as NiO^- and $LiCO_3^-$ were successfully used to visualize nickel rich NCM particles and Li_2CO_3 residuals, respectively.[46–48] With the same purpose, powders exposed to air for two weeks were pressed on an aluminum foil substrate and low-angle FIB-craters were prepared using xenon plasma as shown in Figure 4g. Later, this low-angle crater was examined with ToF-SIMS in imaging-mode (combined with delayed extraction analyzer settings) to obtain cross-section images with chemical information. The relative intensities of $LiCO_3^-$ ion fragments (shown in red) are significantly higher on inter-particle regions and thus reveal the presence of lithium carbonates on NCM particles (it should be noted that the inter-particle regions also consist of pores and therefore the signal intensities can vary between different regions).

In summary, the experimental results of ambient air storage in Figure 4 show that the Li_2O, which may form on the NCM surface during the synthesis or post-synthesis heat treatment, reacts with ambient air (i.e., CO_2 and H_2O) and forms Li_2CO_3 as the main RLC component. The reaction of Li_2O is completed in a few days, however, the growth of Li_2CO_3 continues with increasing air storage time due to ongoing reactions between the NCM surface and the ambient air. Therefore, in order to comprehensively understand the impact of ambient air storage on electrochemical performance, it is crucial to consider not only the formation of Li_2CO_3/LiOH (along with associated near-surface NCM alterations) but also the influence of gradually diminishing (and ultimately vanishing) Li_2O residuals.

Figure 5a–c presents the galvanostatic cycling results of In/InLi–NCM cells featuring NCM samples before and after heat treatment, and after ambient air exposure. In order to obtain information about the degree of electrolyte side reactions and oxidation of RLCs, a deliberate decision was made to perform low current cycling for an easier observation of such

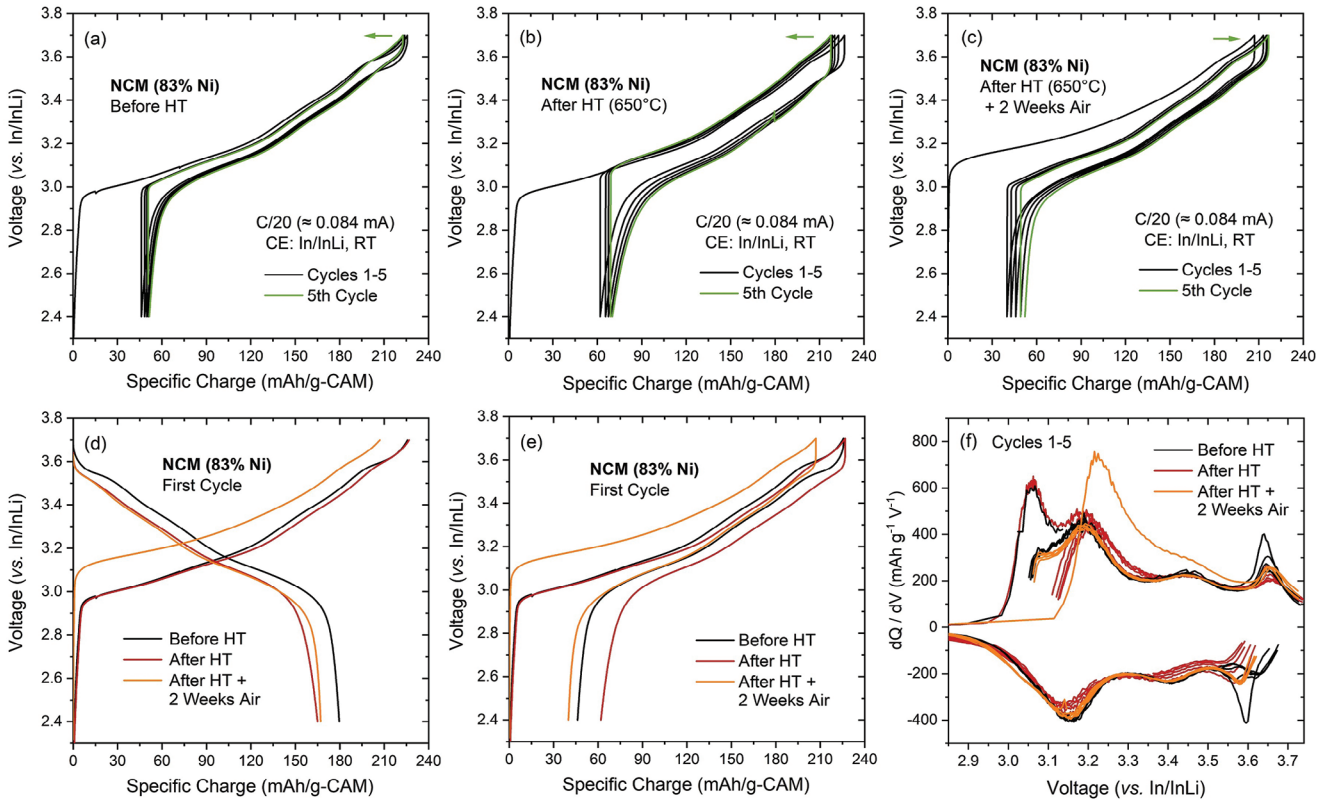

Figure 5. Galvanostatic cycling results of In/InLi-NCM cells with NCM powders; a) before heat treatment, b) after heat treatment, and c) after heat treatment followed by 2 weeks ambient air exposure. In d), first cycle charge and discharge voltage curves are shown in a format more commonly used in the literature so that the charge and discharge capacities begin from zero in each respective curve. In e), the same curves as in (d) are shown in the format preferred in this study so that the charge and discharge currents make a positive and negative contribution to the specific charge, respectively. f) Overlayed differential capacity plots of the data presented in (a–c).

reactions – as well as to obtain more meaningful Coulomb efficiency values. It is seen in Figure 5b that the heat treatment considerably increases the voltage hysteresis and decreases the discharge capacity. Interestingly, the comparison of the voltage profiles during the first charging step (Figure 5d) reveals relatively similar overpotentials and almost the same charge capacity for both cells. However, the overpotential is rather high during discharge for the heat-treated sample. This results in a lower discharge capacity and decreases the first cycle Coulomb efficiency from 0.796 (before heat treatment) to 0.727. It is known that nickel rich NCM-type layered oxides show a kinetic hindrance at low potentials during discharge, and this results in a low Coulomb efficiency in the first cycle.[49] As compared to conventional LiBs with liquid electrolytes, chemo-mechanical effects and associated contact loss at the active material interface may exacerbate the first cycle discharge capacity loss in ASSBs. It is seen that the heat treatment at 650°C causes a further drop in the first cycle Coulomb efficiency which is a result of the asymmetric overpotential observed particularly for this cell during discharge. In following cycles, the capacity retention is also negatively affected by the heat treatment which mainly seems to arise from a negative "charge end point slippage" during charging and a positive "discharge end point slippage" during discharging (an indication of kinetics-related losses during both charge and discharge).

After two weeks of ambient air exposure of the heat-treated sample, a considerable increase in overpotential is observed during charging in the first cycle (see Figure 5d). However, discharge curves and capacities are quite similar before and after air exposure. In Figure 5d, the charge and discharge curves are plotted in a format more commonly used in the literature (i.e., both charge and discharge curves start from zero and increase gradually). On the other hand, when the same data is presented in a hysteresis-type plot (see Figure 5e), the discharge voltage profiles of these two cells look quite different, and samples exposed to ambient storage seem to show a lower overpotential. This is overlooked in the plot in Figure 5d due to start of the profiles from unmatching state of charges (SOCs). Indeed, the Coulomb efficiency increases to 0.807 from 0.727, and as seen in Figure 5c, the voltage hysteresis decreases considerably in the following cycles. As such an unusually high charge overpotential is only limited to the first charge, the charge capacity gradually recovers in subsequent cycles causing a positive "charge end point slippage". During discharge steps, a positive end point slippage is also observed but this is mainly a direct result of positive slippage during charging since no significant drop in discharge capacities is observed in the subsequent cycles. The differential capacity plots in Figure 5f further corroborate the positive effect of ambient air storage on the electrochemical performance (despite an unusual charging behavior only seen in the first cycle).

In light of these findings, it is evident that the electrochemical performance in sulfide-type ASSBs is adversely affected by the heat treatment of nickel-rich NCM powder. However, a significant recovery of this performance loss can be achieved if the same powders are simply exposed to ambient air (e.g., for 2 weeks). Even though the heat treatment conditions were carefully chosen to minimize structural damage, i.e., treatment at 650 °C under pure oxygen flow, it is possible that near-surface regions of the powders could still undergo phase transformations. This is particularly true if these regions experienced partial delithiation during the RCL formation before the heat treatment. However, it is not expected that such structural damages can be recovered through a simple ambient air exposure at room temperature. Therefore, the formation of a Li_2O-rich/Li_2CO_3-deficient surface during heat treatment, and its re-transformation to a Li_2O-deficient/Li_2CO_3-rich surface later during the air exposure, can be considered as a more plausible explanation for the electrochemical performance trends observed in Figure 5. This difference may arise from side reactions caused by Li_2O presence as the correlation to cycling performance seems to align more with Li_2O than with Li_2CO_3 fractions (see Figures S8 and S9, Supporting Information). As discussed in the introduction section, Li_2CO_3 may function as a "natural" protective buffer against side reactions with sulfide SEs, and thus may improve the electrochemical performance.[28–30] For this reason, it is reasonable to investigate the stability of Li_2CO_3 within the operation voltage window of nickel-rich NCMs by more dedicated electrochemical experiments.

2.4. Electrochemical oxidation of Li_6PS_5Cl and Li_2CO_3 – Synthetic charge-discharge profile voltammetry

In LIBs with liquid electrolytes, it has been proposed that Li_2CO_3 can directly be oxidized electrochemically at 3.8 V versus Li^+/Li,[12] or indirectly by chemical reactions when in contact with the electrolyte oxidation products.[14] In ASSBs, if the oxidation of Li_2CO_3 is kinetically feasible to the extent that all Li_2CO_3 residuals are consumed, then a protective role of Li_2CO_3 against electrolyte side reactions would not be expected. Indeed, formation of gaseous products[12] and reactive oxygen species[13] could deteriorate the electrochemical performance due to physical contact loss (e.g., void formation) and deposition of side reaction products at the NCM|SE interface. In order to investigate the effect of Li_2CO_3 on the degree of electrolyte side reactions, and also to study its own electrochemical stability, a modified cyclic voltammetry experiment was performed by using NCM-free composite electrodes consisting of conductive carbon fibers (VGCF) mixed with LPSCl SE (see **Figure 6**a,b) acting as WE against a In/InLi CE. In this experiment, a charge–discharge voltage profile from an actual NCM-based cell is imported to the potentiostat and then a cyclic voltammetry test is performed by mimicking the imported "voltage versus time" data. This electrochemical approach, viz. "synthetic charge-discharge profile voltammetry", has recently been applied to liquid electrolyte cells to study electrolyte oxidation reactions.[50,51] As this approach can enable a better interpretation of voltage curves and Coulomb efficiency values obtained from In/InLi-NCM galvanostatic cycling (e.g., Figure 5), it is preferred over conventional cyclic voltammetry (or linear sweep voltammetry) experiments in this study.

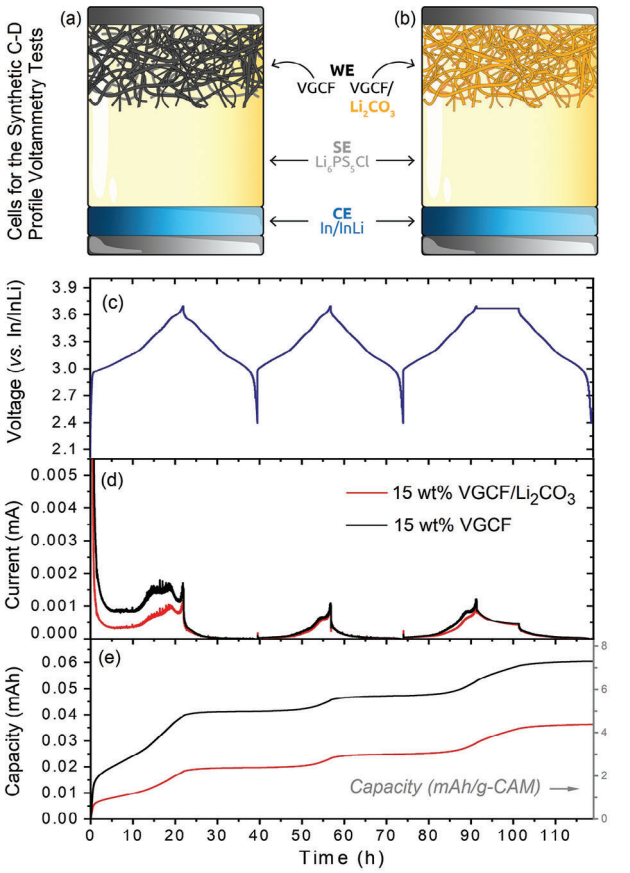

Figure 6. a,b) Schematic drawings of CAM-free cells used in synthetic charge–discharge profile voltammetry tests. c) The voltage profiles imported from an In/InLi-NCM cell were used to polarize a VGCF/LPSCl WE with respect to In/InLi RE/CE. A potentiostatic holding step (10 h) was added in the third cycle at the end of charge. d) The current response of the CAM-free cells during the experiment. e) The accumulated charge (due to oxidation of LPSCl and Li_2CO_3) during the experiment.

As seen in Figure 6d, the In/InLi–VGCF/LPSCl cell exhibits an initial current exceeding 2 µA due to electrolyte side reactions. However, shortly after, the current reduces and stabilizes to nearly 1 µA. As the cell voltage (and voltage scan rate) increases, the current increases again (to nearly 1.5 µA). When Li_2CO_3-coated VGCF is used in the working electrode, a considerable drop in the current is observed in the first cycle during the positive voltage scan (i.e., charging). Interestingly, such a difference in current is not observed in following cycles and the current profiles look similar. Corresponding capacities for these side reactions are also shown in Figure 6e. It is clearly seen that the difference between the two cells primarily arises from the different capacity values obtained in the first cycle. These results suggest that there is no significant Li_2CO_3 (electrochemical) oxidation occurring in the electrode potential window of 2.4 – 3.7 V versus In/InLi (i.e., 3.02 – 4.32 versus Li^+/Li), and in fact, Li_2CO_3 coating seems to mitigate electrolyte oxidation reactions – particularly in the first cycle. These findings indicate that Li_2CO_3 can indeed play a protective role against electrolyte side reactions as

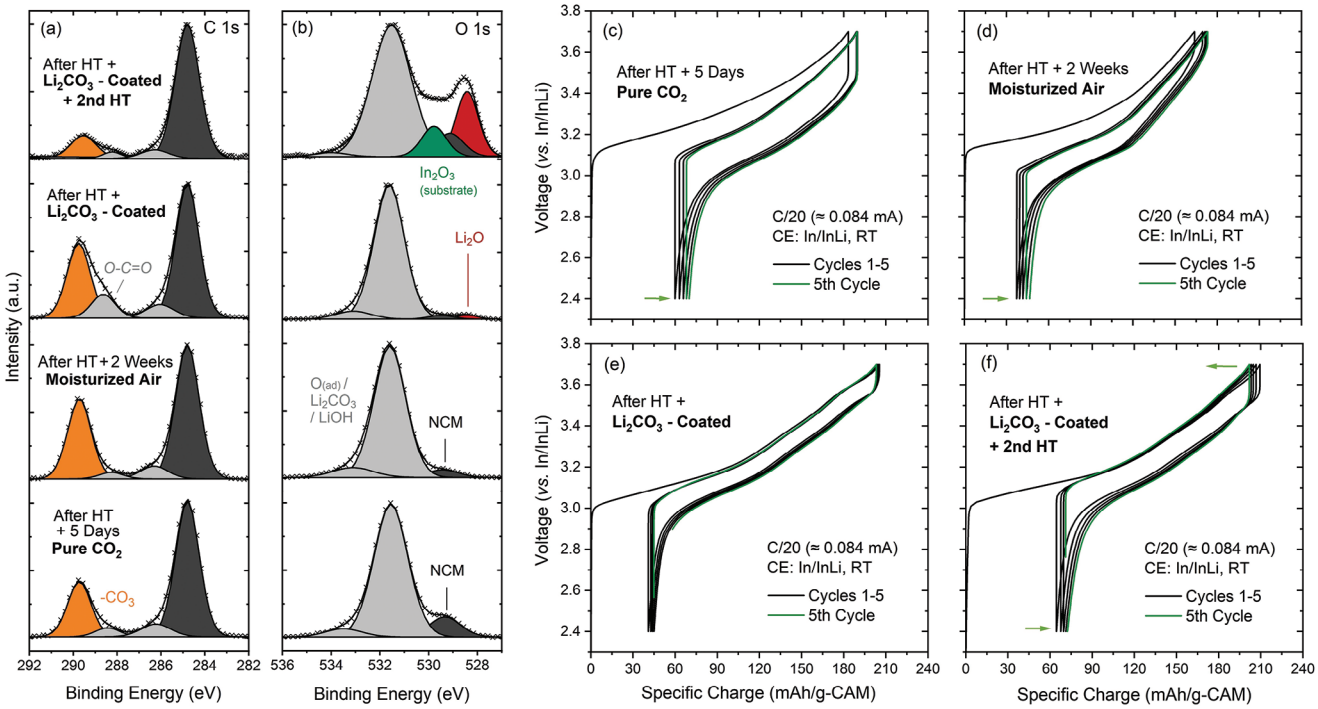

Figure 7. Normalized a) C 1s and b) O 1s XPS spectra of nickel-rich NCM powders stored/heat-treated under different conditions to generate Li_2CO_3 and Li_2O residual lithium compounds on the particle surface. Bare regions of indium metal substrate were visible in the Li_2CO_3-coated + heat treated sample (thus provided an additional energy calibration point). c–f) Galvanostatic cycling results of In/InLi-NCM cells prepared by using NCM powders presented in a,b).

suggested in earlier studies[28–30] and also in a more recently published study.[31] Therefore, the following section reports the impact of various methods and storage conditions which were employed to generate Li_2CO_3 on the NCM-surface.

2.5. Effect of Li_2CO_3 on the NCM surface

As shown in the previous section, Li_2CO_3 does not exhibit significant electrochemical oxidation within the voltage window of a typical NCM-based cell and serves to mitigate LPSCl oxidation side reactions during the initial period of cycling – potentially by acting as a protective layer between the NCM and LPSCl particles. Therefore, it is intriguing to investigate how the formation pathways of Li_2CO_3 on the NCM surface influence the electrochemical performance. For this purpose, the effect of CO_2 exposure was studied first by exposing the heat-treated NCM samples (650 °C, pure O_2) to pure CO_2 gas atmosphere (≈1.4 bar) for 5 days. This resulted in RLC formation of 10.2 mAh g^{-1}-NCM (as determined by acid titration) which consisted of nearly 1.1 wt% Li_2CO_3 and 0.2 wt% LiOH (or ≈0.13 wt% Li_2O). The latter indicates slower Li_2O reaction kinetics in the absence of H_2O in the atmosphere. As seen in **Figure 7**, the presence of Li_2CO_3 is confirmed by the C 1*s* XPS spectrum and no significant intensity is observed for the Li_2O binding energy (i.e., ≈528.6 eV) in the O 1*s* spectrum indicating the conversion of Li_2O to Li_2CO_3 within the surface sensitivity limit of the technique (e.g., < 7–8 nm). The electrochemical performance of cells fabricated using these powders shows a significantly declined performance (see Figure 7c). This can be primarily attributed to the excessive overpotential observed during the charging step. This overpotential is particularly high during the initial charging step resulting in limited charge capacity. Although it diminishes in the subsequent cycle, a substantial voltage hysteresis persists, and this leads to reduced charge and discharge capacities. Interestingly, exposure of the same pristine CAM powder to ambient air for 2 weeks resulted in an improved performance (see Figure 5c) despite having a similar RLC content (12.4 mAh g^{-1}-NCM). Under pure CO_2 atmosphere (due to absence of O_2 and H_2O), instead of a simple delithiation reaction of NCM, formation of Li_2CO_3 via Equation 1 (M = transition metals) requires/causes near-surface transformation from layered NCM to rock-salt phases. It should be noted that these phases (e.g., NiO) are electrochemically inactive and ionically resistive, and addition of O_2 or H_2O into the storage chamber could mitigate/prevent their formation.

$$2\,LiMO_2 + CO_2 \rightarrow 2\,MO + Li_2CO_3 + 1/2\,O_2 \quad (1)$$

In the next step, due to the severe impact of pure CO_2 exposure of NCM on the cell performance, a second batch of powders was prepared for TGA-MS analysis. For this experiment, heat-treated powders were washed with anhydrous methanol and exposed to pure CO_2 for 6 days to generate the same fraction of RLCs as the untreated NCM powders. The TGA-MS results of these powders (as well as the Li_2CO_3-coated and ambient air-stored powders) are shown in Figure S5 (Supporting Information). It is observed that CO_2-exposure shifts the main weight loss and CO_2- release peak to lower temperatures (starting at ≈160 °C). For a better

understanding of the effect of CO_2 exposure on the near-surface structure, future work will be performed (dedicated transmission electron microscopy studies).

In a second storage experiment, NCM powders were stored under moisturized air atmosphere (≈75% rH, 23 °C) for two weeks. The total amount of RLCs was 11.3 mAh g^{-1}-NCM which is attributed to the presence of Li_2CO_3 (≈1.6 wt%). This sample shows similar acid titration results as compared to the sample stored under normal ambient air conditions for the same duration. However, it is evident that high moisture levels have a detrimental impact on the electrochemical performance. Despite displaying similar voltage profiles during the initial stages of charging, after reaching an approximate charge of 100 mAh g^{-1}-NCM, the voltage rapidly rises toward the upper cut-off voltage, thereby limiting the charge capacity. It appears that the unexpected increase in voltage near the end of the charging process cannot be solely attributed to the overpotential since there is not a large voltage hysteresis.

These results clearly show the importance of Li_2CO_3 formation pathways on the electrochemical performance as they show that there is not a simple correlation between the Li_2CO_3 weight fraction in the NCM powder and the cell performance. In storage experiments of NCM that has a low level of Li_2O/LiOH on the surface, the formation of Li_2CO_3 is only possible through the extraction of lithium from the NCM lattice since it is the sole source of lithium. This process can result in near-surface delithiation, structural changes (e.g., rock-salt phase formation), or Li^+/H^+ exchange. In order to investigate the impact of Li_2CO_3 while avoiding these alterations, NCM powders were coated with Li_2CO_3 using an external lithium source (lithium ethoxide solution). After the coating, the total amount of RLCs was 25.2 mAh g^{-1}-NCM with nearly 3 wt% Li_2CO_3 fraction. Despite the large amount of Li_2CO_3 on the surface, the coating process improved the electrochemical performance (see Figure 7e). In the first cycle, even though the charge capacity is slightly lower, the discharge capacity is nearly the same, and the voltage hysteresis is lower as compared to the uncoated sample (see Figure 5b).

These observations indicate a protective role of Li_2CO_3 formed on the NCM particles. On the other hand, there are also strong indications that the presence of Li_2O on the NCM surface could have a negative impact on the cell performance. In order to investigate this possibility further, Li_2CO_3-coated powders were subjected to a second heat treatment at 650 °C. In this experiment, since an external Li source (i.e., precursor for near-surface regeneration) is present on the surface, a positive impact on the cell performance could be expected as the heat treatment could potentially repair the near-surface structure – instead of causing a surface damage during heat treatment. On the other hand, excess Li_2CO_3 could also transform to Li_2O (as observed in Figure 3). As seen in **Figure** 7a,b, this second heat treatment indeed results in a partial transformation of Li_2CO_3 into Li_2O. Electrochemical cycling results show similar charge capacities, but discharge capacities differ considerably due to an asymmetrical overpotential limiting the re-lithiation of NCM. The effect of this asymmetric overpotential on the discharge capacities can be better seen in the overlay voltage-hysteresis type plots from 1st, 2nd, and 5th cycles (see Figure S10, Supporting Information).

These observations necessitate a further investigation to better understand the relative impact of Li_2CO_3 and Li_2O on the CAM

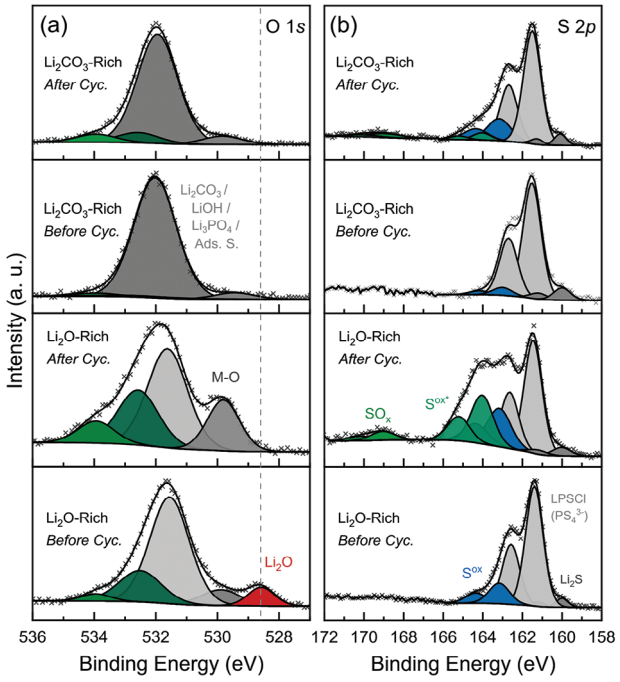

Figure 8. Normalized a) O 1*s* and b) S 2*p* XPS spectra of cathode composites before and after galvanostatic cycling (5 cycles) in cells with In/InLi as counter electrodes.

surface, given the possibility that the difference in cell performance may be mainly driven by Li_2O instead of Li_2CO_3. While the XPS O 1*s* spectra in Figure 7b indicate a conformal Li_2CO_3 coating (as evidenced from the weak metal oxide peak), the second heat treatment induces a transformation to a Li_2O-rich surface and a decline in cycling performance. Additional electrochemical experiments employing ICI[52] and EIS techniques reveal the asymmetric overpotential and internal cell resistance evolution in cells using these samples (see Figure S11, Supporting Information for results and further discussion). Notably, the cell with the Li_2O-rich sample exhibits nearly double the cell resistance of Li_2CO_3-rich sample already after one cycle. The resistance is also highly dependent on SOC and significantly jumps to higher values at high lithiation states. Unlike the Li_2CO_3-rich sample, which shows minimal variation in resistance during charge and discharge, Li_2O-rich samples exhibit strong asymmetric resistance behavior indicating that the direction of current significantly impacts the resistance in this cell.

The post mortem XPS analysis results of these Li_2CO_3-rich and Li_2O-rich samples (after 5 cycles) are shown in **Figure 8** and Figure S12 (Supporting Information). In the initial OCV-state of the Li_2O-rich sample, the O 1*s* spectra clearly show a peak corresponding to the Li_2O binding energy. However, this peak vanishes after cycling, and new peaks indicative of oxygenated sulfur and phosphorus species (e.g., PO_x and SO_x) become visible, however, a definite peak assignment is not possible for these species due to close proximity of binding energy positions of species such as Li_2SO_4 at ≈532.8 eV.[53] Even though such species are also observed in the Li_2CO_3-rich sample, their intensities are rather weak as compared to the Li_2O-rich sample. In the S 2*p* spectra, oxidized sulfur species appear in both samples,

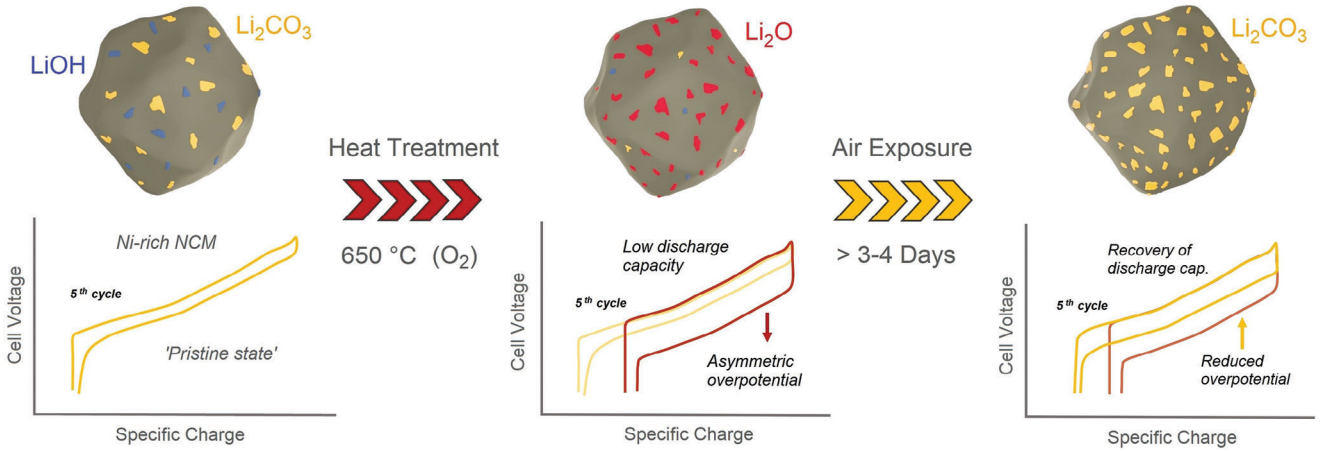

Figure 9. Schematic demonstration (simplified) of single-crystal Ni-rich NCM surface and corresponding slow rate electrochemical cycling performance (e.g. 5th cycle) in In/InLi–NCM cells (with LPSCl solid electrolyte) before/after heat treatment at 650 °C under pure oxygen atmosphere, and before/after subsequent air exposure (e.g. 2 weeks, %rH ≈ 21, T ≈ 22 °C).

however, the Li_2O-rich sample exhibits significantly higher peak intensities. Such species are known to form upon electrochemical oxidation of sulfide-based SEs and attributed to the formation of polysulfides (Li_2S_n), P_2S_n and other oxidized species[46,54,55] which are commonly associated with a decline in electrochemical performance.[56] Presence of oxygenated sulfur species are also visible in S 2*p* spectra as observed at a $2p_{3/2}$ binding energy of ≈169 eV corresponding to sulfate species. Phosphate species were also observed in P 2*p* spectrum of the Li_2O-rich sample at a $2p_{3/2}$ binding energy of ≈133.5 eV (see Figure S12, Supporting Information). Formation of phosphates and sulfates/sulfites at the NCM | LPSCl interface due to reactions between NCM (oxygen source) and LPSCl (phosphorus/sulfur source) is possible,[53] however, it is important to consider the presence of reactive RLCs such as Li_2O also as a potential source of oxygen.

In summary, these results highlight the importance of considering the presence of Li_2O and its detrimental effect when evaluating the influence of residual lithium compounds (RLCs) on the cell performance (see **Figure 9** for a simplified schematic demonstration of single-crystal Ni-rich NCM surface and corresponding electrochemical performance trends upon Li_2O formation and its reaction with air resulting in Li_2CO_3 formation).

3. Conclusions

Formation of RLCs on nickel-rich NCM single crystal particles has been investigated aiming to understand their impact on sulfide-based ASSB performance. Through the utilization of various analytical methods, it is shown that lithium carbonate constitutes the main component of RLCs in samples exposed to air. Even though high temperature treatment of particles leads to substantial gas release (e.g., CO_2), it does not necessarily result in the removal of RLCs. Instead, the overall concentration of RLCs increases during the heat treatment –as accompanied by transformation of other RLCs into Li_2O. It is further shown that subsequent ambient air storage of such powders (i.e., after the heat treatment) not only leads to the formation of new Li_2CO_3 on the surface but also involves the transformation of existing Li_2O into Li_2CO_3 at a relatively fast rate. For these reasons, in order to understand the effect of ambient air storage, it is crucial to consider not only the formation of Li_2CO_3/LiOH (and related near-surface structural alterations), but also the influence of gradually diminishing fraction of Li_2O residuals.

The electrochemical performance of Li_2O-rich heat-treated samples declined, primarily due to an increase in voltage hysteresis resulting from the asymmetric evolution of overpotential during the discharge. This considerably limits the re-lithiation of NCM and thus decreases the discharge capacity. However, this detrimental effect seems to be reversible through ambient air storage. This is partly due to the protective role of Li_2CO_3 which is evidenced by the improved performance of Li_2CO_3-coated NCM electrodes and Li_2CO_3-coated VGCF (i.e., NCM-free) electrodes used as reference-type electrodes. It is important to note that the specific formation conditions of Li_2CO_3 are crucial, as the same beneficial effects are not achieved with pure CO_2 or moisturized air storage. On the other hand, as the secondary heat treatment experiments of Li_2CO_3-coated samples showed, the elimination of Li_2O during air storage may play a more important role than the Li_2CO_3 presence in determining the overall electrochemical performance. In contrast to the general belief that air exposure of nickel-rich NCM oxides should be avoided, short durations of controlled exposure can be beneficial for the performance of sulfide-based ASSB. In any case, the surface state of NCM CAM with respect to RLCs is critical and requires consideration before application.

4. Experimental Section

Materials and Electrolyte: Ni-rich $LiNi_{0.83}Mn_{0.06}Co_{0.11}O_2$ layered oxide powders were purchased from MSE Supplies (micron sized single crystals, $D \geq 1$ µm, trace amounts of B and Zr were found at the surface as determined by X-ray photoelectron microscopy). Single crystal powders were used due to their morphological and structural stability which were not only advantageous for ASSBs[32] but also for liquid electrolyte-based LiBs[33,34] during their long-term cycling. The stoichiometry of powders was confirmed by energy dispersive X-ray spectroscopy. Vapor-grown

carbon fibers (VGCF, Sigma–Aldrich) were used in composite electrodes as conductive (electronic) additive. The CAM powder was washed with deionized (DI) water (in-house), anhydrous ethanol or anhydrous methanol (Sigma Aldrich). The NCM powders (in alumina boats) were heat treated at different temperatures (650, 750, and 800 °C) for 10 h under different atmospheres (pure O_2 flow at 100 sccm flow rate, or ambient air). Synthetic Li_2CO_3 coating of CAM powders and VGCF conductive additives was achieved according to the lithium ethoxide coating approach as reported in an earlier study.[35] Storage experiments were done under ambient air conditions at room temperature (average temperature and relative humidity are given for each specific sample in the related sections). Additional storage experiments were also performed under highly humid air (> 75% rH), and pure CO_2 (0.1 MPa) atmospheres. For the CO_2 experiment, we transferred the powders into a vessel which can be sealed and connected by an adapter to a Swagelok-type custom-built set-up consisting of pressure-gauge, vacuum-line and CO_2-line. All CAM powders were dried in a Büchi vacuum oven at 100 °C for 10 h prior to use in cells. Li_6PS_5Cl (LPSCl) SE powders were purchased from NEI Corporation (ionic conductivity $\sigma_{ion} \approx 1.4$ mS cm^{-1} at 25 °C). The indium foil used in the counter electrode (CE) preparation was 100 µm thick (chemPUR, Germany), and the lithium foil was 200 µm thick (two 100 µm thick foils were hand-pressed, China Energy Lithium). Foils were punched into 9 and 4 mm discs for indium and lithium, respectively.

X-Ray Diffraction (XRD): Measurements of Ni-rich NCM powders were performed in Bragg-Brentano geometry using a PANalytical Empyrean 2 Cu-K_α diffractometer. Samples were exposed to ambient air for less than 1 h during measurements. The measurement range was $15° \leq 2\theta \leq 70°$, and the GSAS-II program was used for the Rietveld refinements.

Thermogravimetric Analysis – Mass Spectrometry (TGA-MS): Measurements were performed with the instrument NETZSCH STA-409-PC coupled with a mass spectrometer QMS 403 Aëolos under argon (50 mL min^{-1}) or a mixture of synthetic air (30 mL min^{-1}) and argon (20 mL min^{-1}). Samples (15–25 mg) were heated up to 800 °C and subsequently cooled down with a rate of 5 °C min^{-1}. For selected samples, two heating/cooling cycles were performed.

Acid Titration: An automatic titrator (SI Analytics TitroLine 7000) with 0.01 M HCl was used to quantify the amount of RLCs dissolved into CAM washing solutions. For each sample, ≈250 mg CAM powder was added into 20 ml DI water (degassed under vacuum prior to use) and stirred for 3 min. The solution was vacuum filtered quickly and additional 140 ml DI water (vacuum degassed) were added to the CAM-free transparent washing solution. This solution was titrated with 0.1 ml acid dosing with 10 s waiting time steps. During titration, the analyte was stirred continuously, however, the stirring rate was carefully adjusted in order to prevent any vortex formation (which could result in CO_2 uptake). Determination of the $LiOH/Li_2CO_3$ ratio was made by evaluating the relative positions of equivalence points (determined from the maxima of derivative curves) as described in previous studies.[4,7] However, it should be noted that any Li_2O impurity present on the CAM could also contribute to the LiOH amount estimated from this titration analysis since water is used both in washing solutions and analyte. Additionally, microwave plasma atomic emission spectroscopy (MP-AES) measurements were performed (with the instrument Agilent 4210) to quantify the elements present in the selected CAM washing solutions which were used for the acid titration. In order to increase the quantification accuracy, measurements were done using an internal calibration approach by adding known amounts of nickel ($NiCl_2 \cdot 6H_2O$), carbon (Li_2CO_3) and lithium (LiCl) salt solutions (at different concentrations) to the analyte.

Electrochemical Testing: Cathode composites were prepared by mixing (hand mixing in mortar for 15 min) of CAM:SE:VGCF in 70:25.5:4.5 weight ratio. All preparation steps were run in an argon glovebox (MBraun, 0.1 ppm < $p(O_2)/p$ and $p(H_2O)/p$ < 1 ppm). 90 mg of LPSCl was used for the separator layer. As CE, lithium or In/InLi electrodes were used. The latter was prepared by hand pressing of 4 mm diameter lithium (200 µm thick) on 9 mm diameter indium foil (100 µm thick). Cells were prepared in a press-cell set up (10 mm diameter) and the cathode composite loading was ≈12 mg ($q_A \approx 2.1$ mAh cm^{-2}). Cells were pressed under 3 tons using a hydraulic press prior to addition of CE. After pressing, the CE was attached to the other side of the separator and the cells were sealed. During testing, aluminum frames were used to apply ≈70 MPa uniaxial electrode stack pressure. All cells were rested for 10 h prior to the start of electrochemical tests (25°C). For the "potentio profile importation" (PPI) tests, i.e., synthetic charge-discharge profile voltammetry, cell voltage versus time data was obtained from galvanostatic test of an In/InLi–NCM cell. Later, these data were imported to the potentiostat and used to mimic the same voltage versus time profile in a modified cyclic voltammetry experiment in which a CAM-free cell was used instead of the actual In/InLi–NCM cell. This CAM-free cell consisted of composite VGCF/LPSCl as the working electrode (WE) and In/InLi as the CE. The CAM-free VGCF/LPSCl electrode had the same mass loading of VGCF as in the CAM:SE:VGCF electrodes. Galvanostatic cycling of cells was performed using a Maccor Series 4000, and PPI tests were performed using a Biologic VMP-300 or VMP-3 potentiostat.

Electron Microscopy: CAM powders were pressed (using a hand press in an argon glovebox) on aluminum foils and then transferred to a scanning electron microscope (SEM) equipped with a field emission gun (Merlin, Carl Zeiss) using a Leica VCT500 air-tight transfer module. Unless specified, measurements were performed at 3 kV operation voltage and 200 pA current. Similarly prepared samples were plasma etched at low angles (e.g., 10° from the sample surface plane) using a FIB/SEM instrument (XEIA3 Triglav, Xe-Plasma FIB, Tescan Orsay Holding). Unless specified, the samples were cooled to –130 °C during plasma etching.

X-Ray Photoelectron Spectroscopy: First, samples were pressed on indium foils by hand, and afterwards, attached on the XPS sample holder using electronically non-conductive adhesive tapes. The sample holder was transferred without air exposure from glovebox to a PHI5000 Versa Probe II or Versa Probe IV system (Physical Electronics GmbH). Monochromated Al-K_α radiation (1487.6 eV, 200 µm beam diameter and 50 W power) was used in measurements (with dual beam charge compensation). The pass energy was 29.35 eV, the step size was 0.25 eV and step time was 50 ms. Casa XPS was used for the evaluation of results. The hydrocarbon peak positioned at E_B(C 1s) = 284.8 eV was used for binding energy calibration. The data are presented after Shirley background subtraction (powder samples) and intensity normalization (divided by the maximum). In peak fittings, a Gaussian/Lorentzian peak shape GL (30) was used.

Time-of-Flight Secondary Ion Mass Spectrometry (ToF-SIMS): Samples were prepared similarly to XPS samples and then transferred to an IONTOF M6 Hybrid SIMS equipped with a 30 kV Bi cluster primary-ion gun. An airtight Leica VCT500 transfer module was used for the transfer. A gas cluster ion beam (Ar_{1500}^+ cluster ions, 10 kV) was used for surface cleaning. Unless specified, the negative ion mode was used in the measurements. A flood gun was used for charge neutralization. "Delayed mode" analyzer settings and "imaging mode" primary ion gun settings were used for image acquisition.

Supporting Information

Supporting Information is available from the Wiley Online Library or from the author.

Acknowledgements

This work had received funding from the Bundesministerium für Bildung und Forschung (BMBF) within the FestBatt – Cluster of Competence for Solid–State Batteries (FB2-Char, 03XP0433D). Cathleen Poetzsch was acknowledged for her help in MP-AES measurements and Raffael Ruess for valuable discussions. Elisa Monte was acknowledged for the illustrations of the graphical abstract and the synthetic charge–discharge profile voltammetry setup.

Open access funding enabled and organized by Projekt DEAL.

Conflict of Interest

The authors declare no conflict of interest.

Author Contributions

B.A., A.H. and J.J. conceived the research idea. B.A. designed the research project and performed experiments, performed acid titration, XPS, XRD, SEM, FIB/SEM, ToF-SIMS measurements/analysis, and TGA-MS analysis. A.E.S. and K.M-B. performed (and contributed to) TGA-MS measurements (analysis). A.H. contributed to the ToF-SIMS analysis. B.A. wrote the whole manuscript and J.J. edited the manuscript. All authors read the manuscript and contributed to it with useful discussions.

Data Availability Statement

The data that support the findings of this study are available from the corresponding author upon reasonable request.

Keywords

air stability of NCM, lithium carbonate, lithium-oxide, LPSCl, Ni-rich NCM, residual lithium

Received: October 25, 2023
Revised: January 3, 2024
Published online: January 31, 2024

[1] W. Li, E. M. Erickson, A. Manthiram, *Nat. Energy* **2020**, *5*, 26.
[2] J. Choi, N. Voronina, Y.-K. Sun, S.-T. Myung, *Adv. Energy Mater.* **2020**, *10*, 2002027.
[3] M. Jiang, D. L. Danilov, R. Eichel, P. H. L. Notten, *Adv. Energy Mater.* **2021**, *11*, 2103005.
[4] A. R. Schuer, et al., *J. Power Sources* **2022**, *525*, 231111.
[5] J. Kim, H. Lee, H. Cha, M. Yoon, M. Park, J. Cho, *Adv. Energy Mater.* **2018**, *8*, 1702028.
[6] R. Jung, R. Morasch, P. Karayaylali, K. Phillips, F. Maglia, C. Stinner, Y. Shao-Horn, H. Gasteiger, *J. Electrochem. Soc.* **2018**, *165*, A132.
[7] Y. Kim, H. Park, J. Warner, A. Manthiram, *ACS Energy Lett.* **2021**, *6*, 941.
[8] W. Zhang, C. Yuan, J. Zhu, T. Jin, C. Shen, K. Xie, *Adv. Energy Mater.* **2023**, *13*, 2202993.
[9] W. M. Seong, Y. Kim, A. Manthiram, *Chem. Mater.* **2020**, *32*, 9479.
[10] Y. Bi, Q. Li, R. Yi, J. Xiao, *J. Electrochem. Soc.* **2022**, *169*, 020521.
[11] I. Hamam, N. Zhang, A. Liu, M. B. Johnson, J. R. Dahn, *J. Electrochem. Soc.* **2020**, *167*, 130521.
[12] S. E. Renfrew, B. D. McCloskey, *J. Am. Chem. Soc.* **2017**, *139*, 17853.
[13] L. A. Kaufman, B. D. Mccloskey, *Chem. Mater.* **2021**, *33*, 4170.
[14] A. T. S. Freiberg, J. Sicklinger, S. Solchenbach, H. A. Gasteiger, *Electrochim. Acta* **2020**, *346*, 136271.
[15] H. Liu, Y. Yang, J. Zhang, *J. Power Sources* **2007**, *173*, 556.
[16] D. Pritzl, T. Teufl, A. T. S. Freiberg, B. Strehle, J. Sicklinger, H. Sommer, P. Hartmann, H. A. Gasteiger, *J. Electrochem. Soc.* **2019**, *166*, A4056.
[17] L. Zhang, E. A. Müller Gubler, C.-W. Tai, Ł. Kondracki, H. Sommer, P. Novák, M. El Kazzi, S. Trabesinger, *ACS Appl. Mater. Interfaces* **2022**, *14*, 13240.
[18] B. Huang, D. Liu, K. Qian, L. Zhang, K. Zhou, Y. Liu, F. Kang, B. Li, *ACS Appl. Mater. Interfaces* **2019**, *11*, 14076.
[19] L. Hartmann, D. Pritzl, H. Beyer, H. A. Gasteiger, *J. Electrochem. Soc.* **2021**, *168*, 070507.
[20] L. Hartmann, C. H. Ching, T. Kipfer, M. Koch, H. A. Gasteiger, *J. Electrochem. Soc.* **2022**, *169*, 070516.
[21] J. Lee, T. Lee, K. Char, K. J. Kim, J. W. Choi, *Acc. Chem. Res.* **2021**, *54*, 3390.
[22] Y. Lu, et al., *Matter* **2022**, *5*, 876.
[23] D. J. Lee, J. Jang, J.-P. Lee, J. Wu, Y.-T. Chen, J. Holoubek, K. Yu, S.-Y. Ham, Y. Jeon, T.-H. Kim, J. B. Lee, M.-S. Song, Y. S. Meng, Z. Chen, *Adv. Funct. Mater.* **2023**, *33*.
[24] H. Visbal, S. Fujiki, Y. Aihara, T. Watanabe, Y. Park, S. Doo, *J. Power Sources* **2014**, *269*, 396.
[25] T. Bartsch, et al., *ACS Energy Lett.* **2018**, *3*, 2539.
[26] T. Hatsukade, A. Schiele, P. Hartmann, T. Brezesinski, J. Janek, *ACS Appl. Mater. Interfaces* **2018**, *10*, 38892.
[27] A. A. Delluva, J. Kulberg-Savercool, A. Holewinski, *Adv. Funct. Mater.* **2021**, *31*.
[28] F. Strauss, S. Payandeh, A. Kondrakov, T. Brezesinski, *Materials Futures* **2022**, *1*, 023501.
[29] J. Kim, O. Kim, C. Park, G. Lee, D. Shin, *J. Electrochem. Soc.* **2015**, *162*, A1041.
[30] A. Y. Kim, et al., *Sci. Rep.* **2021**, *11*, 1.
[31] S. Kang, H.-S. Kim, J. Y. Jung, K.-H. Park, K. Kim, J. H. Song, J.-S Yu, Y.-J. Kim, W. Cho, *ACS Appl. Mater. Interfaces* **2023**, *15*, 10744.
[32] R. Ruess, D. Gomboso, M. A. Ulherr, E. Trevisanello, Y. Ma, A. Kondrakov, T. Brezesinski, J. Janek, *J. Electrochem. Soc.* **2023**.
[33] A. Mesnier, A. Manthiram, *J. Electrochem. Soc.* **2023**, *170*, 080509.
[34] H. Li, et al., *Chem. Mater.* **2019**, *31*, 7574.
[35] A.-Y. Kim, F. Strauss, T. Bartsch, J. H. Teo, T. Hatsukade, A. Mazilkin, J. Janek, P. Hartmann, T. Brezesinski, *Chem. Mater.* **2019**, *31*, 9664.
[36] J. Sicklinger, M. Metzger, H. Beyer, D. Pritzl, H. A. Gasteiger, *J. Electrochem. Soc.* **2019**, *166*, A2322.
[37] A. C. Martinez, *J. Power Sources* **2020**, *468*.
[38] L. De Biasi, B. Schwarz, T. Brezesinski, P. Hartmann, J. Janek, H. Ehrenberg, *Adv. Mater.* **2019**, *31*, 1900985.
[39] N. V. Faenza, L. Bruce, Z. W. Lebens-Higgins, I. Plitz, N. Pereira, L. F. J. Piper, G. G. Amatucci, *J. Electrochem. Soc.* **2017**, *164*, A3727.
[40] S. Payandeh, F. Strauss, A. Mazilkin, A. Kondrakov, T. Brezesinski, *Nano Research Energy* **2022**, *1*, 9120016.
[41] H. Liu, Y. Yang, J. Zhang, *J. Power Sources* **2006**, *162*, 644.
[42] A. Laurita, L. Zhu, P.-E. Cabelguen, J. Auvergniot, J. Hamon, D. Guyomard, N. Dupré, P. Moreau, *ACS Appl. Mater. Interfaces* **2022**, *14*, 41945.
[43] J. Shi, P. Li, K. Han, D. Sun, W. Zhao, Z. Liu, G. Liang, K. Davey, Z. Guo, X. Qu, *Energy Storage Mater.* **2022**, *51*, 306.
[44] T. Oda, Y. Oya, R. U. Olivares, S. Tanaka, *Fusion Eng. Des.* **2006**, *81*, 613.
[45] H. A. Mosqueda, C. Vazquez, P. Bosch, H. Pfeiffer, *Chem. Mater.* **2006**, *18*, 2307.
[46] F. Walther, F. Strauss, X. Wu, B. Mogwitz, J. Hertle, J. Sann, M. Rohnke, T. Brezesinski, J. Janek, *Chem. Mater.* **2021**, *33*, 2110.
[47] Y. You, H. Celio, J. Li, A. Dolocan, A. Manthiram, *Angewandte Chemie – International Edition* **2018**, *57*, 6480.
[48] S.-K. Otto, Y. Moryson, T. Krauskopf, K. Peppler, J. Sann, J. Janek, A. Henss, *Chem. Mater.* **2021**, *33*, 859.
[49] A. Liu, et al., *J. Electrochem. Soc.* **2021**, *168*, 070503.
[50] A. Mathew, M. Lacey, D. Brandell, *Journal of Power Sources Advances* **2021**, *11*, 100071.
[51] E. R. Østli, A. Mathew, J. R. Tolchard, D. Brandell, A. M. Svensson, S. M. Selbach, N. P. Wagner, *Batter Supercaps* **2023**, *6*.
[52] M. J. Lacey, *ChemElectroChem* **2017**, *4*, 1997.
[53] F. Walther, R. Koerver, T. Fuchs, S. Ohno, J. Sann, M. Rohnke, W. G. Zeier, J. Janek, *Chem. Mater.* **2019**, *31*, 3745.
[54] J. Auvergniot, *Solid State Ion* **2017**, *300*, 78.
[55] D. H. S. Tan, *ACS Energy Lett.* **2019**, *4*, 2418.
[56] F. Walther, S. Randau, Y. Schneider, J. Sann, M. Rohnke, F. H. Richter, W. G. Zeier, J. Janek, *Chem. Mater.* **2020**, *32*, 6123.